Macromolecules

ARTICLE

pubs.acs.org/Macromolecules

Real-Time Structure Changes during Uniaxial Stretching of Poly(ω-pentadecalactone) by *in Situ* Synchrotron WAXD/SAXS Techniques

Jiali Cai,[†] Benjamin S. Hsiao,*[,‡] and Richard A. Gross*[,†]

[†]NSF I/UCRC for Biocatalysis and Bioprocessing of Macromolecules, The Polytechnic Institute of New York University, Six Metrotech Center, Brooklyn, New York 11201, United States

[‡]Department of Chemistry, Stony Brook University, Stony Brook, New York 11794, United States

ABSTRACT: Poly(ω-pentadecalactone) (PPDL), a model polymer in the poly(ω-hydroxyl fatty acids) family, is a new biopolymer with monomer synthesized by yeast-catalyzed ω-hydroxylation of fatty acids. In this study, deformation-induced structural changes in two PPDL samples with different molecular weights were studied by *in situ* wide-angle X-ray diffraction (WAXD) and small-angle X-ray scattering (SAXS) techniques. The high molecular weight PPDL (PPDL-high) sample exhibited notable strain hardening, while the low molecular weight PPDL (PPDL-low) sample did not. The behavior can be explained by the entanglement density concept. The evolution of crystallinity (from WAXD) as a function of strain could be divided into four distinct regions, but their respective mechanisms differ slightly in each sample. During stretching, a mesomorphic phase formed in both samples, bridging between the amorphous and strain-induced crystal phases. The SAXS data verified the effect of molecular weight (or the entanglement density) on the deformation-induced structure of PPDL. The parameters of chain orientation factor (f) calculated from the orthorhombic crystal cell as well as the nonorthorhombic crystal cell proposed by Wilchinsky were used to follow the orientation process during stretching of PPDLs. It was found that the different molecular entanglement network (i.e., PPDL-low versus PPDL-high) led to different crystal orientation behavior, especially in the low strain range.

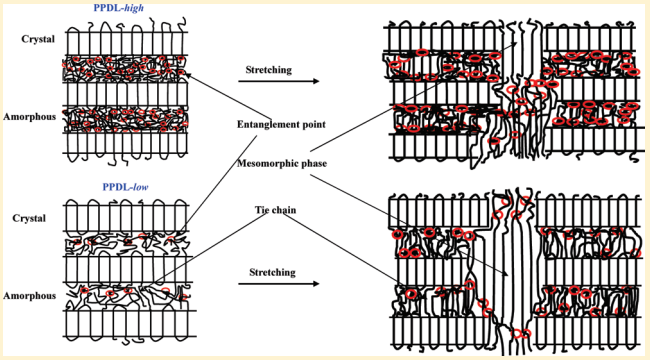

INTRODUCTION

It is well-known that the deformation-induced structure change in semicrystalline polymers can allow the manipulation of mechanical properties.[1−5] Upon deformation, the isotropic structure of polymeric materials can be transformed into an anisotropic structure due to the orientation of polymer chains. Hence, the mechanisms of such transformations and how they are related to the resulting morphology, structure, and physicomechanical properties are of great scientific interest and practical importance in polymer science.[1−3] It is also understood that when crystalline polymers are in the molten state, chains are entangled in a dynamic manner. As the temperature is reduced, some chains can crystallize and the entanglement points are excluded from the crystalline domains and become concentrated in the interlamellar amorphous regions.[6] Thus, the concentration and distribution of chain entanglements in interlamellar amorphous regions would affect the final mechanical properties.[7,8] The mechanical properties of semicrystalline polymeric materials are also influenced by crystallinity, crystalline structure and morphology, amorphous chain orientation, distribution, and concentration of tie chains in the interlamellar amorphous regions.[4,5,7,8] A great number of mechanisms have been proposed to correlate the structure and property relationships. For example, Peterlin[9,10] reported that isotactic polypropylene (iPP) spherulites can be transformed into oriented fibrils above its yield point by passing through stages of elastic deformation, plastic deformation, fragmentation of lamellar structure, and formation of a fibrillar structure upon stretching. Based on another viewpoint, the deformation mechanism in semicrystalline polymers can also include interlamellar and intralamellar slipping of superstructure, chain pull-out from folded-chain lamellae (sometimes termed mechanically induced melting), and recrystallization to form oriented extended-chain crystals.[1,10−14] For example, Strobl et al.[15] argued that the tensile deformation of semicrystalline polymers can be viewed as a stretching of interpenetrating networks of crystalline domains (blocks). In his model, crystalline blocks can slip at small strains, resulting in disintegration and recrystallization above a critical stress. During deformation of certain polymers, polymorphic transformations can also take place.[16−22] The metastable crystal structure prevails under strained conditions because of reduced entropy. This behavior has been observed for iPP,[16−18] PET,[19−21] and PLA.[22] Hsiao et al.,[18] based on the experimental results of iPP, proposed the concept of "entanglement-induced tie chains" and hypothesized that the existence of chain entanglements in interlamellar amorphous regions affects the tie chain

Received: December 28, 2010
Revised: March 13, 2011
Published: April 26, 2011

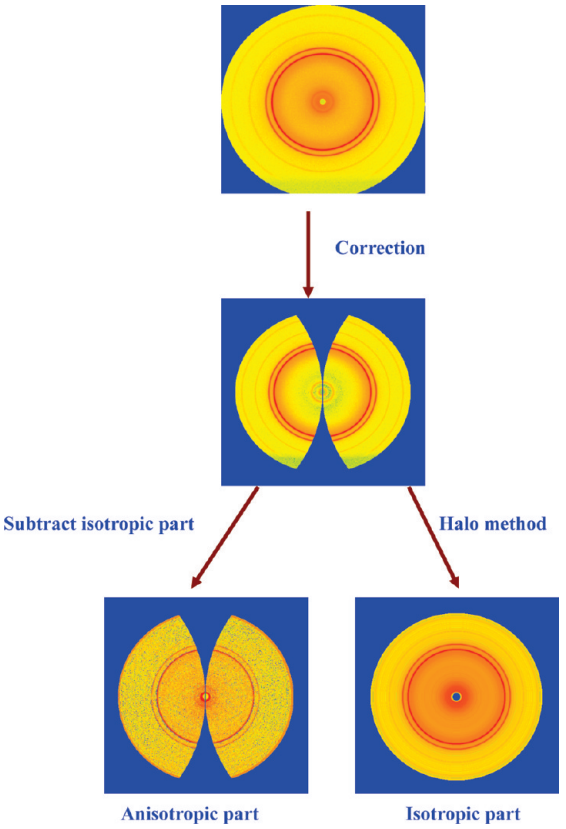

Figure 1. Deconvolution of isotropic and anisotropic contributions from a Fraser-corrected 2D WAXD pattern.

distribution, where the strength of the entanglement network can influence the stability of adjacent crystalline lamellae. They hypothesized that, at low temperatures, entanglements can be considered frozen due to low chain mobility; at high temperatures, disentanglement may occur during stretching by chain slippage. This concept was supported by the observation of strain-induced mesomorphic phase at lower temperatures but not at high temperatures during iPP stretching.

For ductile semicrystalline polymers, the engineering stress–strain curve usually exhibits four regions. Manson et al.[23] assigned these four regions as (I) linear and nonlinear viscoelasticity, (II) neck region/strain softening, (III) plastic flow, and (IV) strain hardening. Many studies on the strain hardening behavior have been carried out[7,25−29] from theoretical and experimental perspectives. They all indicate that the molecular entanglement network dictates the strain hardening behavior. For example, Kennedy and Mandlekern et al.[30,31] contend that the upsweep behavior in the stress–strain curve is mainly due to strain-induced crystallization orientation.

Poly(ω-hydroxy fatty acids), P(ω-OHFAs), have structures similar to polyethylene (PE) but with ester groups separated by generally 13−17 methylene (CH_2) units, dependent on the chain length from which ω-OHFAs are derived. P(ω-HOFAs) can retain the biodegradability in bioactive environments while sharing the common problems of existing bio-based materials (e.g., poly(lactic acid) and microbial polyesters) such as hydrolytic stability, shelf life, and brittleness.[32−34] P(ω-HOFAs) can also overcome the shortcomings of PE, such as low surface chemical reactivity that results in poor adhesion in laminates, blends (e.g., with polyamides and polyesters), and composite materials.[35−37] However, ω-OHFAs are difficult and expensive to prepare by traditional organic synthesis, limiting their usage in commodity materials. A recent report by us describes the engineering of diploid yeast *Candida tropicalis* to produce commercially viable yields of ω-hydroxy fatty acids.[38] In one experiment, volumetric yields exceeding 160 g/L of 14-hydroxytetradecanoic acid (ω-OHC14) during a 140 h fermentation was obtained.

Poly(ω-pentadecalactone) (PPDL) is an excellent model polymer for poly(ω-hydroxyl fatty acids) since it has 14 methylene units between ester moieties along the chain. The component ω-pentadecalactone (PDL) is currently synthesized by a tedious chemical route from petrochemical feedstocks and is primarily manufactured for use in fragrances.[39] A convenient route to synthesize PPDL is via lipase-catalyzed ring-opening polymerization.[40−43] Previous studies in our laboratory with collaborators have investigated the PPDL crystal structure,[44] crystallization and morphology,[45] and mechanical properties.[42,46]

In the present study, two PPDL samples differing in molecular weight (M_n = 40 000, M_w/M_n = 2.7; M_n = 204 000, M_w/M_n = 1.6) were synthesized and investigated to determine their deformation mechanism during uniaxial stretching. The stress–strain curves of these two molecular weight PPDL samples differ each other in that a strain-hardening region before fracture was observed in higher M_n PPDL, but not in lower M_n PPDL. In order to gain a better understanding of the deformation behavior of P(ω-HOFAs), work performed herein using lower and higher M_n PPDL focused on elucidating the changes in morphology and crystal structure during uniaxial stretching by using simultaneous synchrotron wide-angle X-ray diffraction (WAXD) and small-angle X-ray scattering (SAXS) techniques. Important insights resulting from this work include how the mesomorphic phase can bridge the transformation between crystal and amorphous phases during stretching. Furthermore, the molecular entanglement network was found to play a dominant role in the deformation mechanism at room temperature. The deformation behavior of PPDL and high-density polyethylene (HDPE)[46] were further compared due to their structural similarity.

EXPERIMENTAL SECTION

Materials. Samples of ω-pentadecalactone (PDL, 98%) and anhydrous *p*-xylene (>99%) were purchased from Aldrich Chemical Co. and were used as received. Chloroform was purchased from PHARMCO-AAPER Inc. (>99.9%). Anhydrous toluene (98%), purchased from Aldrich Chemical Co., was dried over sodium and then distilled under nitrogen. Novozym 435 (specific activity 10 000 PLU/g) was provided by Novozymes (Bagsvaerd, Denmark) and consisted of *Candida Antarctica* Lipase B (CALB) adsorbed within the macroporous resin Lewatit VPOC 1600 (poly[methyl methacrylate-*co*-butyl methacrylate], supplied by Bayer).

Sample Preparation. The experimental method for PPDL synthesis was the same as that described elsewhere,[40,41,46,47] except for the following modifications: The reaction temperature was increased from 70 to 85 °C, the magnetic stirrer was changed to a glass overhead stirrer, predried 3 Å sieves was added to the reaction mixture, and the round-bottom flask and glass stirrer bar were flame-dried before adding monomer and toluene solvent.

GPC Characterization. Molecular weight of PPDL samples was determined by gel permeation chromatography (GPC) using the Waters HPLC system, where the procedures has been described elsewhere.[41,46]

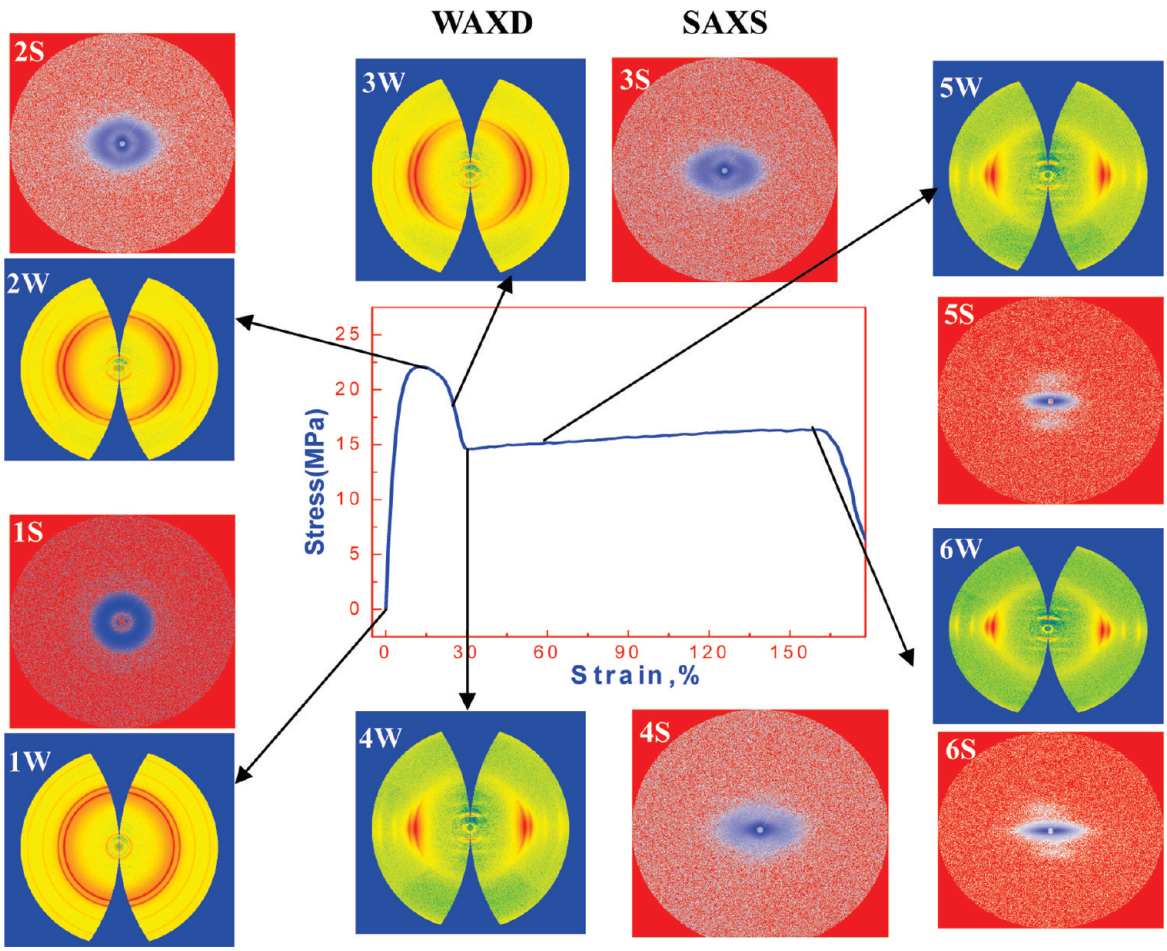

Figure 2. Engineering stress−strain curve and selected 2D SAXS and WAXD patterns acquired during uniaxial tensile deformation of PPDL-low.

The number-average molecular weight (M_n) and weight-average molecular weight (M_w) were determined based on a calibration curve generated by narrow molecular weight polystyrene standards (Aldrich Chemical Co).

Characterizations of WAXD and SAXS during Uniaxial Stretching. *In situ* wide-angle X-ray diffraction (WAXD) and small-angle X-ray scattering (SAXS) measurements were carried out at the X27C beamline in the national Synchrotron Light Source (NSLS), Brookhaven National laboratory (BNL). The wavelength of the synchrotron radiation was 0.1371 nm. A three-pinhole collimation system was used to reduce the beam size to 0.6 mm in diameter. Two-dimensional (2D) WAXD and SAXS patterns were collected by using a Mar CCD X-ray detector (MAR-USA), having a resolution of 1024 × 1024 pixels (pixel size = 158.44 μm). The typical image acquisition time was 15 s for each data frame. The sample-to-detector distance was 1924 mm for SAXS (calibrated by a silver behenate (AgBe) standard) and 116 mm for WAXD (calibrated by an aluminum oxide (Al_2O_3) standard). All X-ray images were corrected for background scattering, air scattering, and beam fluctuations.

Uniaxial tensile deformation was performed using a modified Instron 4442 tensile apparatus, which stretched the sample bar symmetrically. The symmetric stretching ensured that the focused X-ray beam could illuminate the same sample position during deformation. Dumbbell-shaped sample bars with dimensions of 20.0 mm (length) × 4.0 mm (neck width) × 1.5 mm (thickness) were prepared by press-molding at 130 °C and subsequent quenching to ambient temperature. A constant deformation rate of 2 mm/min was applied to the specimen throughout the deformation study at 25 °C. The Merlin software was used to collect and analyze the tensile results. The stress and strain mentioned in this study were all engineering stress and engineering strain.

X-ray Data Analysis. Semiquantitative SAXS analysis was performed to determine the changes of lamellar structure (e.g., long period spacing) during stretching from the meridionally projected scattering peaks.[48] For WAXD analysis, emphasis was given to the phase structure change and crystal orientation. All 2D WAXD patterns were first corrected by the Fraser method to compensate for the effect of flat-plate detection[49] and were then corrected for background (including air) scattering. The corrected pattern was deconvoluted into two parts, isotropic and anisotropic contributions, using the "halo method" (Figure 1).[50] The isotropic contribution can be attributed to unoriented species, including amorphous and unoriented crystal phases, while the anisotropic contribution can be attributed to oriented species, including oriented mesomorphic and crystal phases. The principle for this deconvolution approach is that the azimuthally independent component in the total scattered profile is directly proportional to the unoriented fraction of the scatterer, which can be determined as follows. For each azimuthal scan at a specific scattering angle (2θ), the minimum value of the intensity profile is considered as the envelope intensity of the unoriented species at that angle. By extracting all the minimum values at all scattering angles, a 2D image of the isotropic contribution is generated. This isotropic contribution is then subtracted from the total scattering image, yielding the oriented contribution. Assuming that stretched samples have cylindrical rotation symmetry and the 2D pattern can contain the complete information to describe the intensity

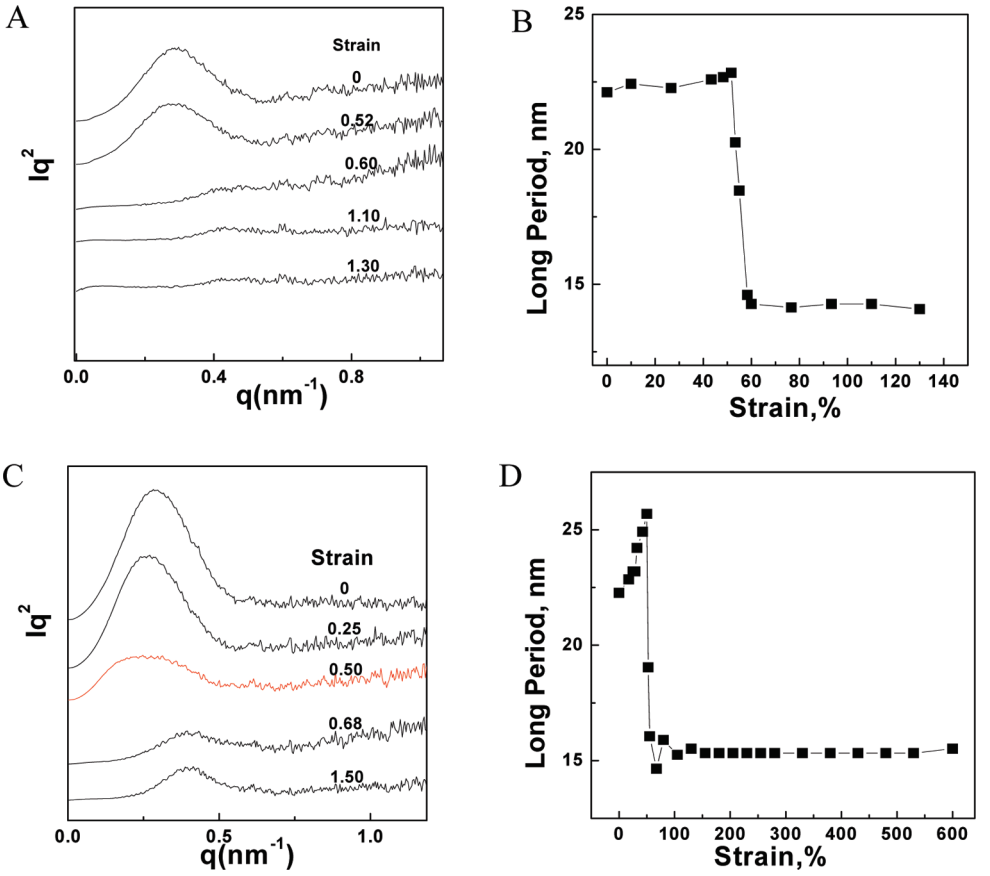

Figure 3. Projected linear SAXS intensity profiles (Iq^2 vs q) along the meridional direction at different strains during uniaxial tensile deformation of PPDL-low (A) and PPDL-high (C) and corresponding changes of the long period as a function of strain for PPDL-low (B) and PPDL-high (D).

distribution in reciprocal space, integration over such 2D sections through 3D reciprocal space will produce the fractions of all phases. The anisotropic fraction was circularly averaged into a linear intensity profile, which was deconvoluted into crystal and oriented mesomorphic phase fractions by using the method of one-dimensional peak fitting. The same method was also applied to analyze the isotropic contribution, where fractions of unoriented crystal and amorphous phases were obtained. The total crystallinity index (hereafter termed crystallinity, since they are proportional to each other) was estimated by the sum of the fractions from oriented and unoriented crystal phases.

RESULTS

Uniaxial Stretching of PPDL M_n = 40 000 (PPDL-low). Figure 2 illustrates the engineering stress−strain curve of PPDL-low during uniaxial tensile deformation at room temperature (25 °C), together with selected 2D-WAXD and SAXS patterns collected at different applied strains. It is seen that the orientation of the initial sample was low. In the initial 2D WAXD pattern, five nearly isotropic diffraction rings were detected, which were indexed (from inner to outer) as (001), (110), (200), (120), and (020) reflections according to the published pseudo-orthorhombic crystal structure of PPDL.[44] The corresponding SAXS pattern also exhibited a nearly isotropic ring, indicating the existence of a lamellar structure with very low orientation. This observation is in agreement with the existence of spherulitic structure observed by AFM.[45] The long period, that is, the average distance between adjacent lamellae, was estimated from the projected scattering peak position of the Iq^2 vs q plot ($= 2\pi/q_{max}$, see Figure 3A).[48] The estimated long period at room temperature before deformation was 21.4 nm.

Necking and plastic flow were observed during stretching. In the stress−strain curve, stress first reached the maximum value at strain 14% (i.e., the yield point) and then decreased, followed by stable propagation before fracture. When the sample length reached 262% of the initial length, the sample bar fractured. The strain-hardening phenomenon was not observed for this relatively low molecular weight PPDL sample.

The corresponding 2D WAXD patterns changed rapidly after the yield point. The azimuthal spreads of all isotropic diffraction rings narrowed while diffraction widths broadened, most notably along the equator. The azimuthal spreads of the (110) and (200) reflection peaks at different strains are shown in parts A and C of Figure 4, respectively, indicating a rapid change of azimuthal spread before and after the yield point. The linear diffraction intensity profile taken along the equator from WAXD at different strains is illustrated in Figure 5A. Because of the low intensities of (120) and (020) peaks, and the enhanced y-axis scale, only (110) and (200) peaks in the nondeformed sample can be observed in Figure 5A. The intensity of the (110) diffraction peak exhibited rapid and complex changes during stretching in the strain range between 0 and 60%. The intensity first increased, then decreased, and subsequently increased. Above 60%, the intensity of the (110) diffraction peak remained almost constant. For the (200) diffraction peak, its intensity changed to a much lesser extent compared to that of (110); above strain 60%, the (200) intensity also remained constant. The peak broadening and the overlap

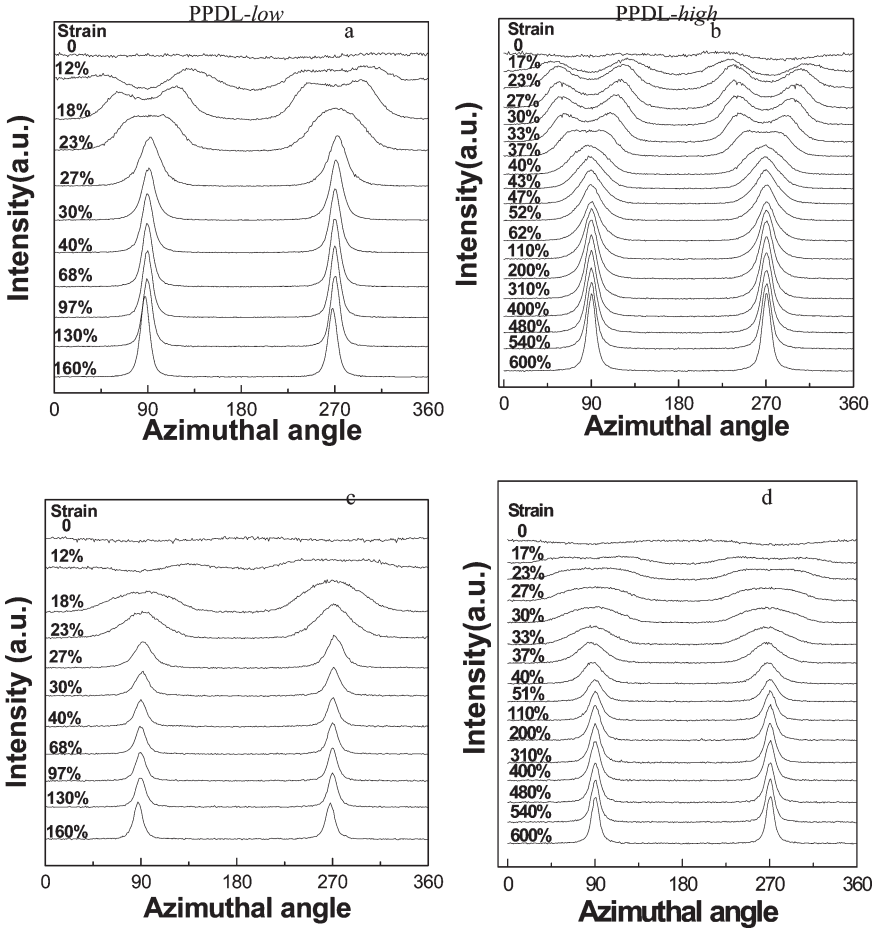

Figure 4. Change of azimuthal profiles of the (110) peak (a, b) and of the (200) peak (c, d) with strain for PPDL-low and PPDL-high, respectively.

between (110) and (200) peaks was observed in the deformed sample (Figure 5A). This can be attributed to the formation of an oriented mesomorphic phase during stretching. Hsiao et al.[18] obtained similar results during investigations of *i*PP uniaxial stretching at 60 °C.

The mass fractions of oriented crystal (OC), unoriented crystal (UOC), oriented mesomorphic (OMP), and amorphous (AP) phases are illustrated in Figure 6A. Interestingly, the total crystallinity (abbreviated as TC, i.e., the sum of oriented crystal and unoriented crystal fractions) with strain can be divided into four regions according to the slope change (I, II, III, IV). The first three regions (I−III) occurred between 0 and 40%, and the IV region spanned between 40% and 160% strain. In region I (0−12%), TC increased slightly and fractions of UOC and AP decreased with strain, while the corresponding fractions of OMP and OC increased. Further analysis indicated that both OC and OMP resulted from AP and reorganization of UOC. In region II (12−25%), TC decreased with strain due to the destruction of formed OC and reduced transformations of the remaining UOC fraction and of AP to OC. The OC fraction first decreased and then increased, and the OMP fraction increased dramatically throughout region II, while both UOC and AP fractions decreased with strain. Numerical calculation indicated that OC, UOC, and AP were transformed into OMP, and the formations of OC and OMP were both derived from UOC and AP. In region III (25−40%), TC and OC fractions increased rapidly with strain, while OMP decreased rapidly and UOC and AP decreased slowly. Thus, in region III, increase of OC is primarily due to transformation of OMP. In region IV (above 40%), the TC fraction increased slightly, accompanied by a small decrease of OMP. Hence, in region IV, a small fraction of OMP was transformed to OC.

In Figure 2, the initial isotropic scattering ring in the SAXS pattern became two-bar like above the yield point, indicating that crystalline lamellae became aligned perpendicularly to the stretching direction. Above strain 60%, the projected scattering intensity was very weak (Figure 3A), which is probably because the density of the crystal phase is very close to that of the oriented mesomorphic phase. The two-bar SAXS pattern on the meridian projected scattering intensity can be explained by the following events:[18] (i) a fraction of lamellar stacks that were parallel (or partially parallel) to the stretching direction were reoriented due to the tendency of chain orientation with stretching; (ii) a fraction of lamellar stacks that were perpendicular (or partially perpendicular) to the stretching direction became fragmented due to the chain pulling-out mechanism. Figure 3B shows that the long period increased slightly from 21.4 to 22.8 nm between strain 0 and 52% and then decreased drastically from 22.8 to 14.3 nm between strain 52% and 60%. The long period increase from 21.4 to 22.8 nm can be attributed to the elastic deformation of PPDL, while the large decrease from 22.8 to 14.3 nm is likely due to rapid strain-induced crystallization coupled with the slippage process between fragmented crystal and strain-induced melting. Above strain 60%, the long period remained almost

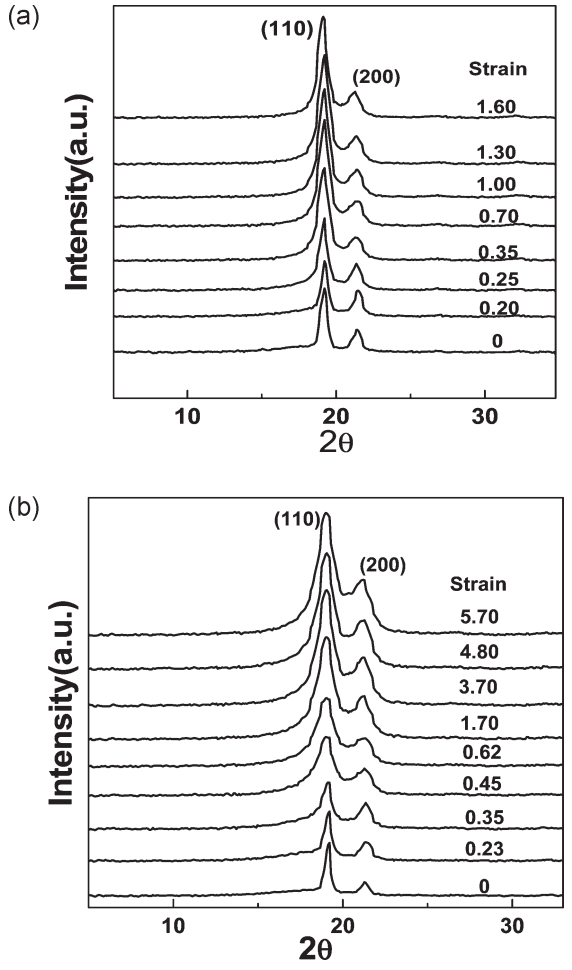

Figure 5. Linear WAXD profiles along the equatorial direction at different strains during the stretching of PPDL-low (a) and PPDL-high (b).

constant. At the later stage of deformation, the SAXS pattern exhibited a strong equatorial streak, consistent with formation of microvoids and strain-induced crystalline fibrils that would occur when for stretched PPDL-low sample bars that fractured at strain 162%.

Uniaxial Stretching of PPDL-high. PPDL-high was subjected to uniaxial stretching at room temperature (25 °C). The resulting engineering stress−strain curve and selected 2D WAXD and SAXS patterns are displayed in Figure 7. Similar to PPDL-low, there was a yield point at strain 18% for PPDL-high. Furthermore, the stress at yield point for PPDL-high was slightly below that of PPDL-low (19 and 22 MPa, respectively). In contrast to PPDL-low, PPDL-high exhibited strain hardening in the stress−strain curve. The initial 2D WAXD of PPDL showed nearly isotropic diffraction rings similar to those of PPDL-low (Figure 2). Also, the corresponding 2D WAXD patterns of PPDL-high changed rapidly after the yield point. In addition, the azimuthal spreads of all isotropic diffraction rings became narrower and the equatorial diffraction peak widths broadened. The azimuthal spreads of the (110) and (200) reflection peaks at different strains are shown in parts B and D of Figure 4, respectively, indicating the rapid change of azimuthal spread before and after the yield point.

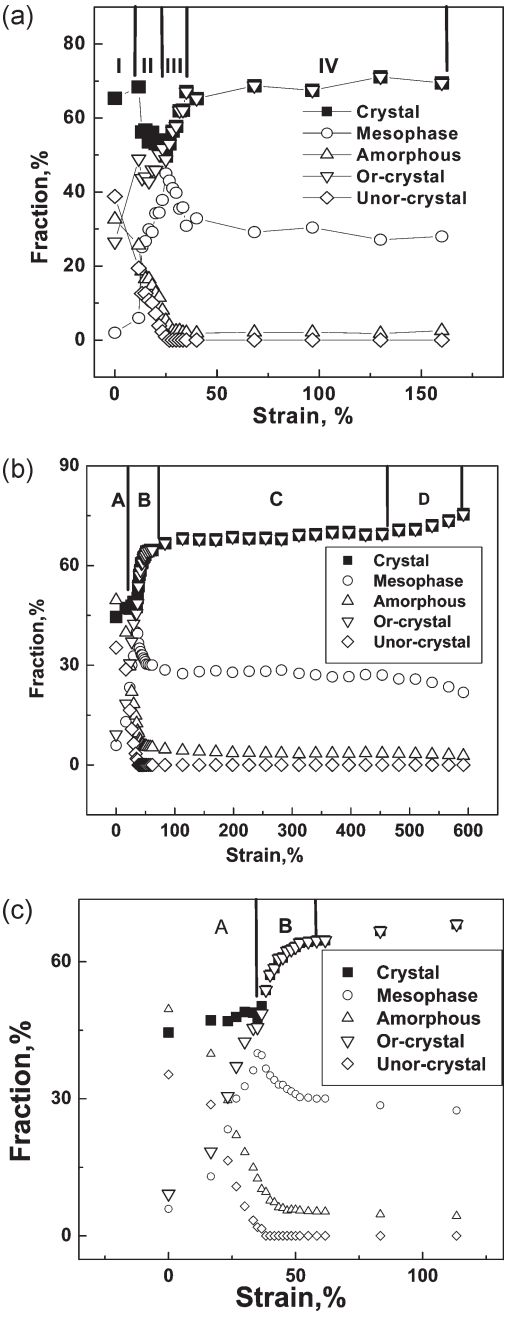

Figure 6. Development of mass fractions of amorphous, mesomorphic, and crystal (including oriented crystal and unoriented crystal) phases in PPDL-low (a) and PPDL-high (b) samples. Plot (c) is an expanded region of plot (b) at low strains.

Figure 5B illustrates the linear WAXD intensity profiles of PPDL-high taken along the equator at different strains. Similar to PPDL-low, only peaks (110) and (200) were considered since the intensities of peaks (120) and (020) were too weak. In contrast to PPDL-low, intensity changes of the PPDL-high (110) diffraction peak with strain exhibited three distinct regions based on observed slope changes. In the strain range between 0 and 0.35, the intensity of (110) diffraction peaks decreased with strain. In the strain range between 0.35 and 1.70, the intensity of (110) diffraction peaks increased rapidly with strain. Above strain 1.70, the increase of intensity was slower until fracture. In

dx.doi.org/10.1021/ma102949h |*Macromolecules* 2011, 44, 3874–3883

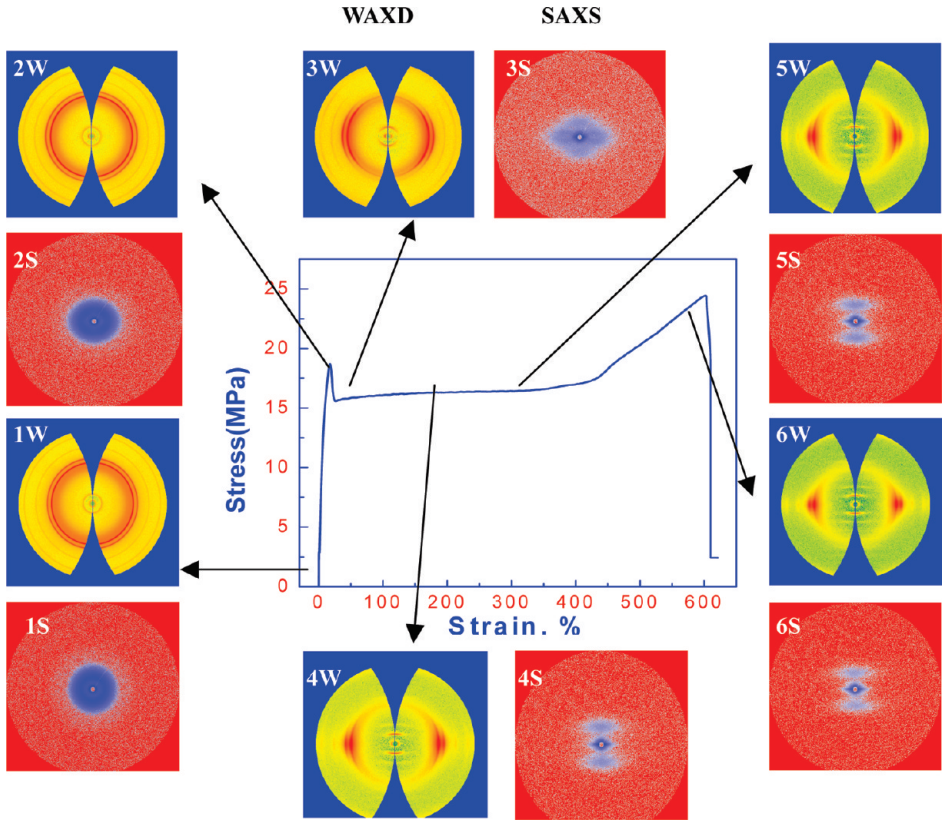

Figure 7. Engineering stress−strain curve and selected 2D SAXS and WAXD patterns acquired during uniaxial tensile deformation of PPDL-high at room temperature.

contrast, intensity changes of the (200) peak with strain exhibited two distinct regions based on observed slope changes. At strains between 0 and 1.70, the intensity increased at a relatively higher rate, while at strains above 1.70, the intensity increase was much slower and close to that of the (110) peak. In addition, peak broadening behavior and the overlap between (110) and (200) peaks were observed with increasing strain, which was similarly observed for PPDL-low, indicating the coexistence of crystal and mesomorphic phases.

Figure 6B illustrates the mass fractions from different phases (OC, UOC, OMP, and AP), where Figure 6C is the enlarged part of Figure 6B at low strains. The total crystallinity (TC) was also divided into four regions according to the slope change, but these four regions differed from those for PPDL-low. To differentiate these four regions with those of PPDL-low, they were labeled as A, B, C, and D. In region A (at strain between 0 and 49%), TC increased slightly with strain and fractions of OC and OMP increased drastically with strain, while fractions of UOC and AP decreased rapidly with strain. Numerical calculations indicated that, in region A, the formation of OC came not only from UOC but also from AP, whereas OMP primarily came from reorganization of UOC and AP. In region B, TC rapidly increased with strain due to the rapid transformation from OMP and AP into OC. In region C, the TC fraction slightly increased with strain, accompanied by a slight decrease in the OMP fraction. In region D, i.e., the strain-hardening region, the slope of TC increased with strain compared with that in region C and the OMP fraction slope correspondingly increased with strain. Interestingly, the TC fraction before fracture of PPDL-high increased from 44.5% to 75.4%. In contrast, for PPDL-low, the TC fraction upon fracture increased from 65.4% to 69.5%. The fractions of the OMP before fracture in PPDL-high and PPDL-low samples were 22.0% and 28.0%, respectively.

Selected 2D SAXS patterns in Figure 7 indicate the rapid change of the scattering maximum above the yield point. The one-dimension meridional projected scattered intensity plots of Iq^2 vs q and the long period change with strain are shown in parts C and D of Figure 3, respectively. Figure 3D indicates that the long period of the initial PPDL-high sample was 22.3 nm; as strain increased from 0 to 50%, the long period increased to 25.7 nm. The increase in the PPDL-high long period was 2.5 times that of PPDL-low within the same strain range. At strain between 50% and 70%, the long period decreased dramatically from 25.7 to 15.3 nm (10.4 nm decrease), whereas PPDL-low decreased by 8.4 nm over the same strain range. At strains above 70%, the long period for both PPDL-low and PPDL-high remained almost constant until fracture.

Crystal Orientation. To compare crystal orientation changes with strain for PPDL-low and PPDL-high, azimuthal angle spreads of (110) and (200) crystal planes of the two samples were selected and the results are shown in Figure 4. Azimuthal angle spreads of (110) and (200) rapidly became narrow, while the crystal orientation of PPDL-low changed more rapidly than that of PPDL-high. The chain orientation factor (f) in the crystal structure was calculated by the Hermans' function (eq 1)[51]

$$f = \frac{3\langle \cos^2 \phi \rangle - 1}{2} \quad (1)$$

where ϕ is the angle between the chain axis and the reference

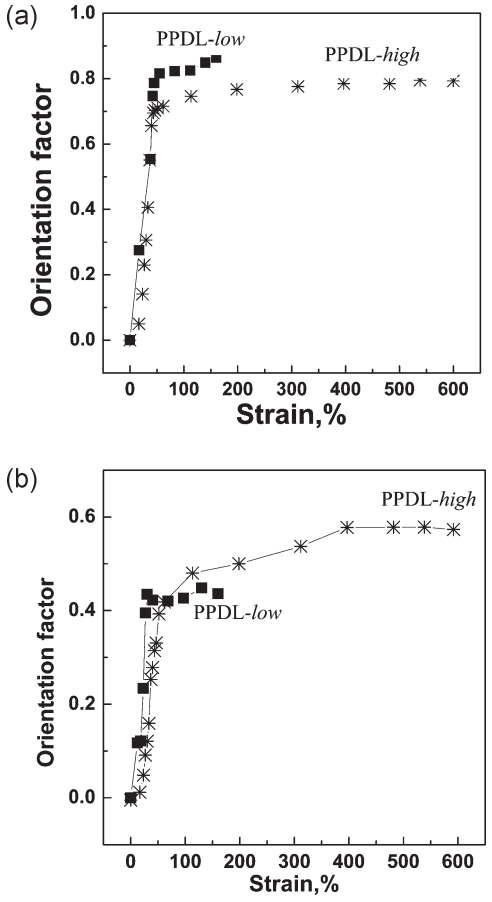

Figure 8. Hermans' orientation factor of the crystal chain axis determined as a function of strain for PPDL-low and PPDL-high, based on (a) nonorthorhombic (from the (110) and (200) diffraction peaks) and (b) orthorhombic (from the (001) diffraction peak) unit cell systems.

axis (stretching direction). The term $\langle \cos^2 \phi \rangle$ is defined as

$$\langle \cos^2 \phi \rangle = \frac{\int_0^{\pi/2} I(\phi) \cos^2 \phi \sin \phi \, d\phi}{\int_0^{\pi/2} I(\phi) \sin \phi \, d\phi} \quad (2)$$

where $I(\phi)$ is the scattered intensity along the angle ϕ. However, since there is no crystal plane of symmetry perpendicular to the PPDL chain axis, Wilchinsky[51−53] suggested that, for nonorthorhombic crystal systems, $\langle \cos^2 \phi \rangle$ can be calculated from (110) and (200) crystal reflections of PPDL using the following expression:

$$\langle \cos^2 \phi \rangle = 1 - 1.452\langle \cos^2 \phi_{110} \rangle - 0.458\langle \cos^2 \phi_{200} \rangle \quad (3)$$

When chains are aligned perfectly along the reference axis, $f = 1$; when chains are aligned perpendicular to the reference axis, $f = -0.5$, and for random orientation, $f = 0$. This formula was proven useful to evaluate the crystal orientation during stretching of PPDL-based copolymers.[54−56] Using eqs 1, 2, and 3, crystal orientation factors of PPDL-low and PPDL-high with strain were obtained, and the results are plotted in Figure 8a. It was found that, at strain below 37%, the crystal orientation factor of PPDL-low was higher than that of PPDL-high. At strain between 37% and 41%, the orientation factors of the two samples coincided. At strain above 41%, the orientation factor of PPDL-low was again higher than that of PPDL-high. Interestingly, although PPDL-high exhibited much higher strain before fracture, the orientation factor of PPDL-low before breaking was still higher than that of PPDL-high before fracture.

DISCUSSION

In our previous work,[44] we determined the crystal structure of PPDL as having a pseudo-orthorhombic monoclinic unit cell with dimensions of $a = 0.749$ nm, $b = 0.503$, $c = 2.000$ nm, and $\beta = 90.06°$. Although PPDL is a polyethylene-like polyester, the (001) diffraction peak of this sample was clearly observed (see Figures 2 and 7, the diffraction ring was close to beam stop). In contrast, for PE, the (001) diffraction peak is seldom observed by WAXD. The appearance of the (001) peak enabled direct calculation of the PPDL crystal orientation factor. Also, this provided a unique opportunity to compare results calculated by using Wilchinsky's method and values obtained from the direct analysis of the (001) crystal plane. Figures 2 and 7 display the changes of the (001) peak azimuthal spread with strain. At high strains, the (001) peak appeared as two parallel lines on the meridian in WAXD patterns. Since $\beta = 90.06°$ in the monoclinic unit cell, we can assume, to a very good approximation, that the PPDL crystal structure is an orthorhombic unit cell and then calculate the orientation factor of PPDL-low and PPDL-high, respectively, according to eqs 1 and 2.[57] The results of these calculations are shown in Figure 8b. Surprisingly, the orientation factor obtained from the orthorhombic crystal system was always less than that obtained from the nonorthorhombic crystal system at the same strain. This indicates that the orientation of different crystal planes along the stretching axis is not necessarily equivalent. In addition, the intensity fluctuation should be considered when analyzing the difference in orientation factors using nonorthorhombic and orthorhombic crystal systems. Since the image acquisition time was short and the intensity of the (001) peak was much lower than those of (110) and (200) peaks, these factors can affect the $\langle \cos^2 \phi \rangle$ calculation using eq 2. In Figure 8b, we observed that at strains less than 40% the crystal orientation factor of PPDL-low was higher than that of PPDL-high and then remained almost constant. However, at strains above 40%, the orientation factor of PPDL-high continued to increase with strain until 400%, leading to a higher c-axis chain orientation before fracture than was observed for PPDL-low. At strains above 400%, the orientation factor of PPDL-high remained almost constant. Comparison of orientation factors of PPDL-high and PPDL-low (Figure 8a,b) indicates that the different molecular entanglement networks of PPDL-low and PPDL-high greatly affected the crystal orientation during stretching, especially in the low strain range (<40%).

Since M_n of PPDL-high was 5 times that of PPDL-low, the initial entanglement points per chain are higher in PPDL-high than those in PPDL-low.[30,31] Schematic diagrams in Figure 9 illustrate the deformation of crystal and amorphous phases during uniaxial tensile deformation for two PPDL samples, differing in chain length. According to the classic rubber-elastic theory,[58] the number of statistical chain segments (N_e) between the cross-linking points can be calculated from the maximum draw ratio (λ_{max}), assuming the effect of crystallinity as physical cross-links is neglected, by the formula $N_e = \lambda_{max}^2$. For PPDL-low and PPDL-high, the average values of N_e are 6.8 and 49,

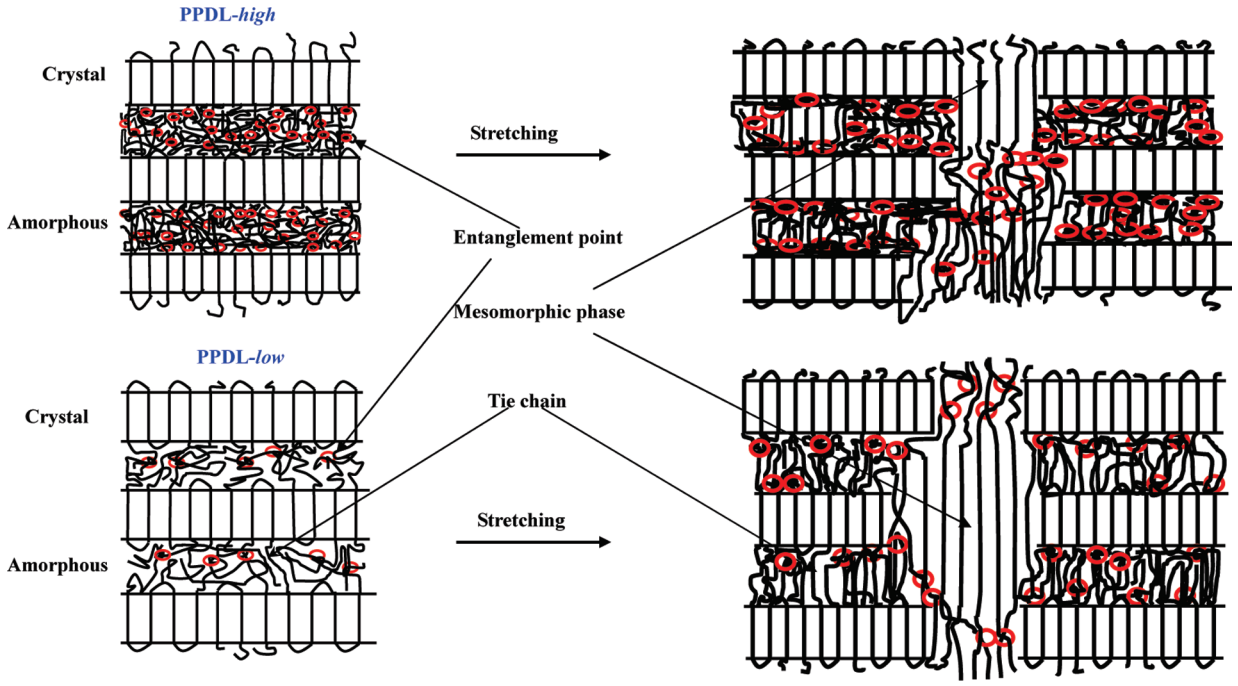

Figure 9. Illustrations of deformation for PPDL-low and PPDL-high crystal and amorphous phases with different entanglement densities during uniaxial tensile deformation.

respectively. Thus, the average chain length between adjacent entanglement points in PPDL-high is 7 times that of PPDL-low. Differences in interlamellar entanglement density can lead to different structure changes upon deformation as was observed herein by WAXD (Figure 6) and SAXS (e.g., the different long periods and their changes in Figure 3B,D).

Mesomorphic phase formation induced by uniaxial stretching was observed for both PPDL-low and PPDL-high samples. Initially, the oriented mesomorphic phase formed simultaneously with orientation of crystals. Upon further deformation, the mesomorphic phase partly transformed into oriented crystal phase. Since transformation of the amorphous phase to oriented mesomorphic phase leads to a large reduction in entropy, this provides an explanation for the rapid decrease in the long period as well as the rapid increase in total crystallinity during deformation. One way to view the mesomorphic phase is it functions as a bridge for transformation between crystal and amorphous phases.

Many theoretical and experimental studies performed[24−29] agree that the molecular entanglement network plays a dominant role in strain hardening behavior. For example, Kennedy and Mandlekern et al.[30,31] argued that the upsweep in the stress−strain curve in semicrystalline polymers, such as high density polyethylene (HDPE), is usually due to strain-induced crystallization behavior. For PPDL-low, the entanglement density is not sufficient to produce strain hardening before fracture. In contrast, for PPDL-high, the higher entanglement density results in strain hardening in the stress−strain curve.

CONCLUSIONS

In this study, *in situ* X-ray experiments were performed to investigate the changes of crystal structure and morphology during deformation of polyethylene-like polyesters, poly(pentadecalactone), PPDL, of different molecular weights were synthesized by enzyme-catalyzed ring-opening polymerization. The X-ray analysis included synchrotron wide-angle X-ray diffraction (WAXD) and small-angle X-ray scattering (SAXS) measurements coupled with uniaxial stretching performed using an Instron instrument.

The high molecular weight PPDL (PPDL-high) exhibited a strain-hardening phenomenon during uniaxial stretching at room temperature (25 °C), while the low molecular weight PPDL (PPDL-low) did not. The results indicate that the average length between the entanglement points (i.e., the entanglement length) is an important factor that affects the structure changes in PPDL during stretching. On the basis of the slope changes, both PPDL-low and PPDL-high plots of total crystallinity with strain could be divided into four regions, which differed in corresponding strain regions. The mesomorphic phase formed during uniaxial stretching reached a maximum value with strain. The mesomorphic phase functions as a bridge for transformations of crystal and amorphous phases during uniaxial stretching. The SAXS results also verified the effect of entanglement density on the deformation-induced structure changes, which are in agreement with the WAXD results.

Although PPDL is a polyethylene-like polyester, the (001) diffraction peak of this sample was clearly observed. In contrast, for PE, the (001) diffraction peak is seldom observed by WAXD. Thus, for PPDL, we had the unique opportunity to compare the results calculated by the Wilchinsky's method and the values obtained from the direct analysis of the (001) crystal plane. Based on methods developed by Wilchinsky, calculation of the chain orientation factors (f) for PPDL-low and PPDL-high samples were made. The results indicate that the orientation processes during uniaxial stretching were different for PPDL-low and PPDL-high. The crystal orientation factors calculated using Wilchinsky's method were comparable with those determined directly from the analysis of the orthorhombic unit cell. Both WAXD results were also in agreement with the crystallinity

analysis from WAXD and the lamellar analysis from SAXS. The above observations further confirm that the different molecular entanglement networks formed in PPDL-low and PPDL-high led to different chain orientation during stretching, especially in the low strain region (<40%).

■ ACKNOWLEDGMENT

The authors thank the National Science Foundation (NSF) and industrial members of the NSF-I/UCRC for Biocatalysis and Bioprocessing of Macromolecules at NYU/Polytechnic University for their financial support, intellectual input, and encouragement during the course of this research. B.H. also thanks the financial support from NSF (DMR-0906512).

■ REFERENCES

(1) Ward, I. M. *Mechanical Properties of Solid Polymers*; John Wiley & Sons: New York, 1983; Chapter 12, p 399.
(2) Hong, K.; Rastogi, A.; Strobl, G. *Macromolecules* **2004**, *37*, 10165.
(3) Men, Y.; Rieger, J.; Homeyer, J. *Macromolecules* **2004**, *37*, 9481.
(4) Yamada, K.; Kamezwa, M.; Takayanagi, M. *J. Appl. Polym. Sci.* **1981**, *26*, 49.
(5) De Rosa, C.; Auriemma, F.; De Lucia, G.; Resconi, L. *Polymer* **2005**, *46*, 9461.
(6) Wunderlich, B. *Macromolecular Physics*; Academic Press: New York, 1976; Vol. 2.
(7) Smith, P.; Lemstra, P. J.; Booij, H. C. *J. Polym. Sci., Part B: Polym. Phys.* **1981**, *19*, 877.
(8) Van Melick, H. G. H.; Govaert, L. E.; Meijere, H. E. H. *Polymer* **2003**, *44*, 2493.
(9) Peterlin, A. *J. Mater. Sci.* **1971**, *6*, 490.
(10) Peterlin, A. *Colloid Polym. Sci.* **1987**, *265*, 357.
(11) Flory, P.; Yoon, D. *Nature (London)* **1978**, *272*, 226.
(12) Popli, R.; Mandelkern, L. *J. Polym. Sci., Part B: Polym. Phys.* **1987**, *25*, 441.
(13) Galeski, A. *Prog. Polym. Sci.* **2003**, *28*, 1643.
(14) De Rosa, C.; Auriemma, F.; De Ballesteros, O. R. *Phys. Rev. Lett.* **2006**, *96*, 167801/1–4.
(15) Men, Y.; Rieger, J.; Strobl, G. *Phys. Rev. Lett.* **2003**, *91*, 095502/1–4.
(16) Ran, S.; Zong, X.; Fang, D.; Hsiao, B. S.; Chu, B. S.; Chu, B.; Philips, R. A. *Macromolecules* **2001**, *34*, 2569.
(17) Ran, S.; Zong, X.; Fang, D.; Hsiao, B. S.; Chu, B. S.; Chu, B.; Cunniff, P. M. *J. Mater. Sci.* **2001**, *36*, 3071.
(18) Zuo, F.; keum, J. K.; Chen, X. M.; Hsiao, B. S.; Chen, H. Y.; Lai, S. Y.; Wevers, R.; Li, J. *Polymer* **2007**, *48*, 6867.
(19) Ran, S.; Wang, Z.; Burger, C.; Chu, B.; Hsiao, B. S. *Macromolecules* **2002**, *35*, 10102.
(20) Kawakami, D.; Ran, S.; Burger, C.; Fu, B.; Sics, I.; Hsiao, B. S. *Macromolecules* **2003**, *36*, 9275.
(21) Kawakami, D.; Hsiao, B. S.; Ran, S.; Burger, C.; Avila-Orta, C.; Sics, I. *Macromolecules* **2005**, *38*, 91.
(22) Mulligan, J.; Cakmak, M. *Macromolecules* **2005**, *38*, 2333.
(23) Manson, J. A.; Hertzberg, R. W. *CRC Crit. Rev. Macromol. Sci.* **1973**, *1*, 433.
(24) Schrauwen, B. A. G.; Janssen, R. P. M.; Govaert, L. E.; Meijer, H. E. H. *Macromolecules* **2004**, *37*, 6069.
(25) G'Sell, C.; Jonas, J. J. *J. Mater. Sci.* **1981**, *16*, 1956 .
(26) G'Sell, C.; Hiver, J. M.; Dahoun, A.; Souahi, A. *J. Mater. Sci.* **1992**, *27*, 5031.
(27) Haward, R. N. *Polymer* **1994**, *35*, 3852.
(28) Capapccio, G.; Gibson, A. G.; Ward, I. M. In *Ultra-High Modulus Polymers*; Ciferri, A., Ward, I. M., Eds.; Applied Science Publ.: London, 1979; p 1.
(29) Smith, P.; Lemstra, P. J. *Colloid Polym. Sci.* **1980**, *258*, 891.
(30) Kennedy, M. A.; Peacock, A. J.; Failla, M. D.; Lucas, J. C.; Mandelkern, L. *Macromolecules* **1995**, *28*, 1407.
(31) Kennedy, M. A.; Peacock, A. J.; Mandelkern, L. *Macromolecules* **1994**, *27*, 5297.
(32) Bhardwaj, R.; Mohanty, A. K. *J. Biobased Mater. Bioenergy* **2007**, *1* (2), 191.
(33) Garlotta, D. *J. Polym. Environ.* **2001**, *9* (2), 63.
(34) Sudesh, K.; Abe, H.; Doi, Y. *Prog. Polym. Sci.* **2000**, *25*, 1503.
(35) Olsson, A.; Lindström, M.; Iversen, T. *Biomacromolecules* **2007**, *8*, 757.
(36) Cole-Hamilton, D. J. *Angew. Chem., Ind. Ed.* **2010**, *49* (46), 8564.
(37) Quinzler, D.; Mecking, S. *Angew. Chem., Ind. Ed.* **2010**, *49* (46), 8564.
(38) Lu, W. H.; Ness, J. A.; Xie, W. C.; Zhang, X. Y.; Minshull, J.; Gross, R. A. *J. Am. Chem. Soc.* **2010**, *132*, 15451.
(39) http://www.bedoukian.com/products/product.asp?id=9100.
(40) Uyama, H.; Takeya, K.; Kobayashi, S. *Bull. Chem. Soc. Jpn.* **1995**, *68*, 56.
(41) Kumar, A.; Kalra, B.; Dekhterman, A.; Gross, R. A. *Macromolcules* **2000**, *33*, 6303.
(42) Focarete, M. L.; Scandola, M.; Kumar, A.; Gross, R. A. *J. Polym. Sci., Part B: Polym. Phys.* **2001**, *39*, 1721.
(43) Simpson, N.; Takwa, M.; Hult, K.; Johansson, M.; Martinelle, M.; Malmström, E. *Macromolecules* **2008**, *41*, 3613.
(44) Gazzano, M.; Malta, V.; Focarete, M. L.; Scandola, M.; Gross, R. A. *J. Polym. Sci., Part B: Polym. Phys.* **2003**, *41*, 1009.
(45) Cai, J. L.; Hsiao, B. S.; Gross, R. A. *Polym. Int.* **2009**, *58*, 944.
(46) Cai, J. L.; Liu, C.; Cai, M. M.; Zhu, J.; Zuo, F.; Hsiao, B. S.; Gross, R. A. *Polymer* **2010**, *51* (5), 1088.
(47) de Geus, M. Enzymatic Catalysis in the Synthesis of New Polymer Architectures and Materials. Ph.D. Thesis, Eindhoven University of Technology, Netherlands, Feb 2007; Chapter 5.
(48) Hsiao, B. S.; Kennedy, A. D.; Leach, R. A.; Chu, B.; Harney, P. *J. Appl. Crystallogr.* **1997**, *30*, 1084.
(49) Fraser, R. D. B.; Macrae, T. P.; Millaer, A.; Rowlands, R. J. *J. Appl. Crystallogr.* **1976**, *9*, 81.
(50) Ran, S.; Zong, X.; Fang, D.; Hsiao, B. S.; Chu, B.; Ross, R. *J. Appl. Crystallogr.* **2000**, *33*, 1031.
(51) Wilchinsky, W. Z. *J. Appl. Phys.* **1969**, *31*, 1960.
(52) Wilchinsky, W. Z. *J. Appl. Phys.* **1959**, *30*, 792.
(53) Wilchinsky, W. Z. *Adv. X-Ray Anal.* **1963**, *6*, 231.
(54) Focarete, M. L.; Gazzano, M.; Scandola, M.; Kumar, A.; Gross, R. A. *Macromolecules* **2002**, *35* (21), 8066.
(55) Ceccorulli, G.; Scandola, M.; Kumar, A.; Kalra, B.; Gross, R. A. *Biomacromolecules* **2005**, *6* (2), 902.
(56) Jiang, Z. Z.; Azim, H. S.; Gross, R. A.; Focarete, M. L.; Scandola, M. *Biomacromolecules* **2007**, *8*, 2262.
(57) Stein, R. S. *J. Polym. Sci.* **1959**, *31*, 327.
(58) Treloar, L. R. G. *The Physics of Rubber Elasticity*, 3rd ed.; Clarendon: Oxford, 1975.